Inorganic Chemistry

pubs.acs.org/IC

Article

Synthesis, Characterization, and Phosphoesterase Activity of a Series of 4f- and 4d-Sandwich-Type Germanotungstates $[(n\text{-}C_4H_9)_4N]_{l/m}H_2[(M(H_2O)_3)(\gamma\text{-}GeW_{10}O_{35})_2]$ (M = Ce^{III}, Nd^{III}, Gd^{III}, Er^{III}, l = 7; Zr^{IV}, m = 6)

Elias Tanuhadi, Emir Al-Sayed, Alexander Roller, Hana Čipčić-Paljetak, Donatella Verbanac, and Annette Rompel*

Cite This: *Inorg. Chem.* 2020, 59, 14078−14084

Read Online

ACCESS | Metrics & More | Article Recommendations | Supporting Information

ABSTRACT: We report on a family of five new 4f- and 4d-doped sandwich-type germanotungstates with the general formula $[(n\text{-}C_4H_9)_4N]_{l/m}H_2[(M(H_2O)_3)(\gamma\text{-}GeW_{10}O_{35})_2]\cdot 3(CH_3)_2CO$ [$M(H_2O)_3(GeW_{10})_2$] (M = Ce^{III}, Nd^{III}, Gd^{III}, Er^{III}, l = 7; Zr^{IV}, m = 6), which have been synthesized at room temperature in an acetone−water mixture. Among the compound series, $[Zr(H_2O)_3(GeW_{10})_2]^{8-}$, which has been obtained in the presence of 30% H_2O_2, represents the first example of a 4d-substituted germanotungstate incorporating the intact dilacunary $[\gamma\text{-}Ge^{IV}W_{10}O_{36}]^{8-}$ building block. All compounds were characterized thoroughly in the solid state by single-crystal and powder X-ray diffraction (XRD), IR spectroscopy, thermogravimetric analysis (TGA), and elemental analysis and in solution by NMR and UV−vis spectroscopy. The phosphoesterase activity of $[Ce(H_2O)_3(GeW_{10})_2]^{9-}$ and $[Zr(H_2O)_3(GeW_{10})_2]^{8-}$ toward the model substrates 4-nitrophenyl phosphate (NPP) and *O*,*O*-dimethyl *O*-(4-nitrophenyl) phosphate (DMNP) was monitored with ^{1}H- and ^{31}P-NMR spectroscopy revealing an acceleration of the hydrolytic reaction by an order of magnitude (k_{corr} = 3.44 (±0.30) × 10^{-4} min^{-1} for $[Ce(H_2O)_3(GeW_{10})_2]^{9-}$ and k_{corr} = 5.36 (±0.05) × 10^{-4} min^{-1} for $[Zr(H_2O)_3(GeW_{10})_2]^{8-}$) as compared to the uncatalyzed reaction (k_{uncat} = 2.60 (±0.10) × 10^{-5} min^{-1}). $[Ce(H_2O)_3(GeW_{10})_2]^{9-}$ demonstrated improved antibacterial activity toward *Moraxella catarrhalis* (MIC 32 μg/mL), compared to the unsubstituted $[GeW_{10}O_{36}]^{8-}$ POM (MIC 64 μg/mL).

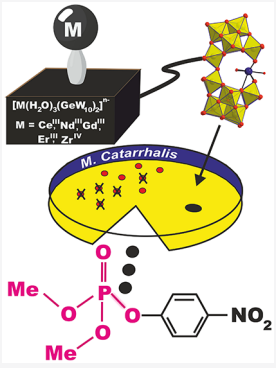

INTRODUCTION

Polyoxometalates (POMs)[1] represent a broad class of anionic inorganic clusters with versatile structural topologies resulting in a variety of chemical and physical properties which can be modulated by molecular design. These features make them attractive materials in a wide range of fields like catalysis,[2,3] electrochemistry,[4] magneto chemistry,[5] and biological chemistry[6,7] including protein crystallography.[8−10] In contrast to plenary POMs, lacunary POMs have well-defined vacant sites and higher negative charges, which make them interesting as multidentate inorganic ligands toward heteroatoms.[11] The combination of Keggin-type lacunary building blocks with heteroatoms has resulted in a broad variety of POM subclasses including triangle-shaped, tetrameric and dimeric sandwich-type POMs, with the latter structural-type being the largest subfamily of heteroatom substituted POMs.[12]

Out of the vast variety of reaction systems using lacunary POMs as precursors, only 18 examples applying Keggin-type lacunary precursors in organic media have been reported to date (Table S1), although undesired isomerization and condensation of POMs commonly encountered in aqueous solution can be circumvented in organic solvents. Among the lacunary building blocks used in organic solvent, the $[(n\text{-}C_4H_9)_4N]_4H_4[\gamma\text{-}Si^{IV}W_{10}O_{36}]$ lacunary POM is the most commonly used precursor.[13,14] The germanium analogue $[(n\text{-}C_4H_9)_4N]_4[\gamma\text{-}Ge^{IV}W_{10}O_{34}(H_2O)_2]$,[15] however, has not been reported in combination with electrophiles, e.g., lanthanides, in organic media yet. Also, the number of 4f-metal substituted germanotungstates which have been prepared remains scarce (Table S2). Most sandwich-type compounds have been studied toward their catalytic properties, such as water oxidation[16] and Mannich-type reactions.[17] Owing to their properties as Lewis acids, 4f- and 4d-doped sandwich-POMs are interesting candidates for hydrolysis reactions.[18]

The high negative charge, water solubility, and solution stability under physiological conditions have made POMs attractive candidates for interaction studies with biological systems.[6] Phosphodiester bonds are characterized by a high stability with a half-life of 130 000 years toward hydrolysis

Received: June 22, 2020
Published: September 18, 2020

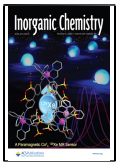

https://dx.doi.org/10.1021/acs.inorgchem.0c01852
Inorg. Chem. 2020, 59, 14078−14084

under physiological conditions, protecting the genetic material.[19] As a matter of fact, attention has been paid to the controlled cleavage of this relatively inert bond as a vital step in biology.[20] Being inspired by nature, the majority of researchers uses Lewis acid containing catalysts as artificial phosphoesterases.[21−23] Based on previous work, lanthanide(III)- and zirconium(IV) ions are highly suitable for designing artificial phosphoesterases, as they exhibit high charge density and coordination number, as well as fast ligand exchange rates.[24] Chemical warfare agents (CWAs), which represent a significant threat to both military and civilian populations, are interesting targets for artificial phosphoesterases as commonly used CWAs such as nerve agents are organophosphorus (OP) esters containing P−X bonds (X = CN, SR). OP nerve agents are highly toxic by inactivating acetylcholinesterase leading to even death in high doses. The primary and effective way for the environmentally friendly decontamination of nerve agents is hydrolysis. The Lewis acidic hydrolysis catalyzed by activation of the phosphorus oxygen bond upon coordination to the Lewis acidic sites has attracted attention as well.[25−27] A series of zirconium(IV) based hydrolytic catalysts including metal oxides, metal hydroxides, and metal−organic frameworks (MOFs) have been reported,[25] but due to their heterogeneous nature, it is difficult to determine the exact structure of active sites. Hence, the development of molecular catalysts with Lewis acidic centers for the homogeneous degradation of nerve agents contributes to understanding the hydrolytic mechanism and crucial factors during the decontamination process. Hill and co-workers thoroughly investigated the Zr-substituted POM, $\{[\alpha\text{-}PW_{11}O_{39}Zr(\mu\text{-}OH)(H_2O)]_2\}^{8-}$, as a homogeneous catalyst for the hydrolysis of a nerve agent and its simulants in a buffered solution. However, the number of studies on POM compounds as homogeneous Lewis acid catalysts for the decontamination of nerve agents remains scarce. Moreover, the applied Zr-POM dimer is unstable and dissociates into its monomeric form under turnover conditions.[28,29] Attributed to their high negative charge, strong acidity, and geometry, POMs have been subjected to antibacterial studies exhibiting synergy with some conventional antibiotics[30] or direct antibacterial activity[31] against both Gram-negative and Gram-positive bacteria. In general, high-nuclear, highly negatively charged POMs exhibit a high activity.[32] *Moraxella catarrhalis* is a Gram-negative human mucosal pathogen, which causes middle ear infections in infants and children and lower respiratory tract infections in adults with chronic pulmonary disease.[32,33] Among the different archetypes tested toward their antibacterial properties, sandwich-type POMs are the most promising representatives.[6]

Herein, we report on the facile synthesis of five new monosubstituted sandwich-type germanotungstates with the general sum formula $[(n\text{-}C_4H_9)_4N]_{l/m}H_2[(M(H_2O)_3)(\gamma\text{-}GeW_{10}O_{35})_2]\cdot 3(CH_3)_2CO$ in the following termed as $[\mathbf{M(H_2O)_3(GeW_{10})_2}]$ (M = Ce^{III}, Nd^{III}, Gd^{III}, Er^{III}; l = 7 and Zr^{IV}; m = 6), which, to the best of our knowledge, represent the first examples of monosubstituted 4f-germanotungstates incorporating the intact dilacunary $\gamma\text{-}[GeW_{10}O_{36}]^{8-}$ building block. $[\mathbf{Ce(H_2O)_3(GeW_{10})_2}]^{9-}$ and $[\mathbf{Zr(H_2O)_3(GeW_{10})_2}]^{8-}$, exhibiting the highest water solubility ($c \sim 5.3$ mM) (Table S19) among the investigated $[\mathbf{M(H_2O)_3(GeW_{10})_2}]$ series, were tested toward their phosphoesterase activity with the model compound 4-nitrophenyl phosphate (NPP) (60 °C, pD = 7.0). Characterized by a higher Lewis activity compared to $[\mathbf{Ce(H_2O)_3(GeW_{10})_2}]^{9-}$, a comprehensive study on the hydrolytic activity of $[\mathbf{Zr(H_2O)_3(GeW_{10})_2}]^{8-}$ toward the nerve agent simulant *O*,*O*-dimethyl *O*-(4-nitrophenyl) phosphate (DMNP) under ambient reaction conditions (25 °C, pD = 7.0) was carried out, and its stability under turnover conditions was confirmed by recyclability experiments and postcatalytic IR spectroscopy. The antibacterial activity of the isostructural polyanions $[\mathbf{Ce(H_2O)_3(GeW_{10})_2}]^{9-}$ and $[\mathbf{Zr(H_2O)_3(GeW_{10})_2}]^{8-}$ was tested against *Moraxella catarrhalis* thereby revealing an enhanced inhibitory effect of the $[\mathbf{Ce(H_2O)_3(GeW_{10})_2}]^{9-}$ polyanion as compared to the unsubstituted $[GeW_{10}O_{36}]^{8-}$ lacunary anion and no inhibitory effect for the pure Ce(III) salt, which highlights the importance of POM lacunary ligands for the enhancement of the antibacterial properties of Lewis acidic metal centers.

RESULTS AND DISCUSSION

Synthesis. The first step in the synthesis of $[\mathbf{M(H_2O)_3(GeW_{10})_2}]$ was the preparation of the lacunary literature known precursor $[(n\text{-}C_4H_9)_4N]_4[\gamma\text{-}GeW_{10}O_{34}(H_2O)_2]$[15] ((TBA)[$GeW_{10}$]) (TBA = tetrabutylammonium). Upon addition of 0.5 equiv of $Ln(acac)_3$ (acac = acetylacetonate; Ln = Ce^{III}, Nd^{III}, Gd^{III}, Er^{III}) and stoichiometric amounts of water to a white suspension of (TBA)-[GeW_{10}] in acetone (Scheme 1), a clear reaction mixture was

Scheme 1. Schematic Representation Showing the Synthesis of $[\mathbf{M(H_2O)_3(GeW_{10})_2}]^{n-}$ Starting from the Dilacunary ((TBA)[GeW_{10}] TBA = Tetrabutylammonium) Precursor[a]

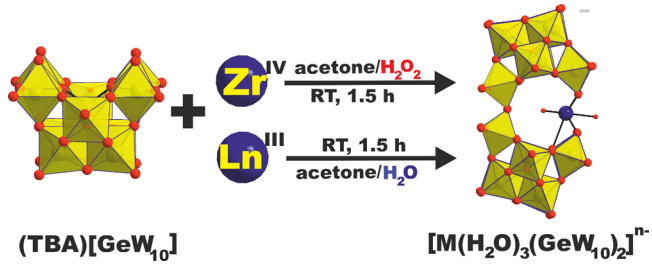

[a]In contrast to the Ln^{III} system, the addition of H_2O_2 to the reaction mixture is crucial for the successful incorporation of Zr^{IV} into the POM architecture (M = Ce^{III}, Nd^{III}, Gd^{III}, Er^{III}, n = 9; Zr^{IV}, n = 8). Blue and red spheres represent the M- and oxygen ions, respectively. Grey for Ge and yellow polyhedra for $\{WO_6\}$.

obtained. It is worth noting that elevated H_2O contents, e.g., to enable the use of pure inorganic $Ln(NO_3)_3$ salts as 4f-metal sources instead of $Ln(acac)_3$, resulted in the partial formation of the Keggin ion $[\alpha\text{-}GeW_{12}O_{40}]^{4-}$ as confirmed by SXRD measurements (CCDC 1915317, Tables S7, S14, and S15). The reaction was carried out under mild conditions in acetone at room temperature (RT). Considering the low stability and high reactivity of $[\gamma\text{-}XW_{10}]$ units (X = Si^{IV}, Ge^{IV}, P^{V}),[34] higher reaction temperatures than RT would have resulted in undesired isomerization and/or partial decomposition of the lacunary units, respectively. After 90 min of stirring and filtration of the reaction mixture at RT, block shaped crystals of $[\mathbf{M(H_2O)_3(GeW_{10})_2}]$ were obtained in yields of 79% $[\mathbf{Ce(H_2O)_3(GeW_{10})_2}]^{9-}$ (CCDC 1915355), 76% $[\mathbf{Nd(H_2O)_3(GeW_{10})_2}]^{9-}$ (CCDC 1915316), 54% $[\mathbf{Gd(H_2O)_3(GeW_{10})_2}]^{9-}$, and 40% $[\mathbf{Er(H_2O)_3(GeW_{10})_2}]^{9-}$ (CCDC 1915318) based on $Ln(acac)_3$ from a mixture of

https://dx.doi.org/10.1021/acs.inorgchem.0c01852
Inorg. Chem. 2020, 59, 14078−14084

acetone and diethyl ether (~5:1, (v/v)) after approximately 1 week.

The first attempts to adapt the synthetic conditions used for the lanthanide incorporating counterparts for the synthesis of 4d sandwiches using zirconium(IV) resulted in the formation of precipitates which despite all our efforts could not be further characterized. It has recently been shown that the reactive peroxide ligand can disassemble Zr_4 square tetramers and cubic hexamers that dominate the solution phase chemistry of zirconium(IV).[35] Considering this regulatory effect of peroxo-ligands, 10 equiv of H_2O_2 were added to a solution of 2 equiv of $Zr(acac)_4$ in acetone followed by the addition of (TBA)[GeW_{10}] (Scheme 1). *Note that acetone/H_2O_2 mixtures should be handled with care due to possible formation of acetone peroxides.* Upon addition of H_2O_2, an immediate color change from colorless to yellow was observed indicating coordination of the peroxo-ligands to the Zr^{IV} ions. Filtration of the reaction mixture after 90 min and addition of diethyl ether (acetone/diethyl ether, 5:1) resulted in the formation of colorless block shaped crystals of $[\mathbf{Zr(H_2O)_3(GeW_{10})_2}]^{8-}$ (CCDC 2010882) in a yield of 65% based on W after approximately 2 weeks.

Structure. Single-crystal X-ray diffraction (SXRD) measurements were performed on $[\mathbf{Ce(H_2O)_3(GeW_{10})_2}]^{9-}$ (Tables S8, S9), $[\mathbf{Nd(H_2O)_3(GeW_{10})_2}]^{9-}$ (Tables S10, S11), $[\mathbf{Er(H_2O)_3(GeW_{10})_2}]^{9-}$ (Tables S12, S13), and $[\mathbf{Zr(H_2O)_3(GeW_{10})_2}]^{8-}$ (Tables S16, S17). All polyanions crystallize in a monoclinic space group ($C_{2/m}$ for $[\mathbf{Ce(H_2O)_3(GeW_{10})_2}]^{9-}$, $[\mathbf{Nd(H_2O)_3(GeW_{10})_2}]^{9-}$, and $[\mathbf{Zr(H_2O)_3(GeW_{10})_2}]^{8-}$ and $P2_1/c$ for $[\mathbf{Er(H_2O)_3(GeW_{10})_2}]^{9-}$). The polyanions are isostructural with idealized C_{2v} point group symmetry. The architecture of $[\mathbf{M(H_2O)_3(GeW_{10})_2}]$ represents a polyanion composed of two [γ-$GeW_{10}O_{35}$]$^{6-}$ lacunary units linked by two oxygen bridging ligands resulting in a "pacmanlike" monolacunary dimer. Occupation of the vacant site with the corresponding heterometal results in the monosubstituted sandwich-type germanotungstate architecture. In all compounds, the metal center exhibits a distorted square antiprism coordination geometry with three H_2O ligands and M−O bond lengths ranging from 2.195(2) to 2.308(2) Å. The three water ligands can be easily exchanged and are a prerequisite for hydrolytic activity (Figure 1). To the best of our knowledge, $[\mathbf{M(H_2O)_3(GeW_{10})_2}]$ represent the first examples of a family with distinct γ-GeW_{10} lacunary units incorporating a 4f- or 4d-metal, respectively (Table S2), which could only be achieved under the ambient reaction conditions preventing the *in situ* isomerization of the lacunary precursor to the monolacunary [β_2-$GeW_{11}O_{39}$]$^{8-}$ building block or the plenary [α-*A*-$GeW_{12}O_{40}$]$^{4-}$ polyanion.[34] Importantly, the successful incorporation of the heteroatoms could exclusively be achieved in organic solution by preventing formation of metal hydroxides commonly encountered in aqueous solution. Despite all efforts, single-crystals of $[\mathbf{Gd(H_2O)_3(GeW_{10})_2}]^{9-}$ with sufficient quality for SXRD measurements could not be obtained. However, elemental analysis and IR spectroscopic investigations (Figure S1) clearly indicate the successful synthesis of pure $[(n\text{-}C_4H_9)_4N]_7H_2[(Gd(H_2O)_3)(\gamma\text{-}GeW_{10}O_{35})_2]$. Powder XRD measurements were performed on compounds $[\mathbf{M(H_2O)_3(GeW_{10})_2}]$ (M = Ce^{III}, Nd^{III}, Er^{III}, and Zr^{IV}) and compared to the corresponding simulated spectra, thereby showing the homogeneity of all bulk compounds (Figure S9).

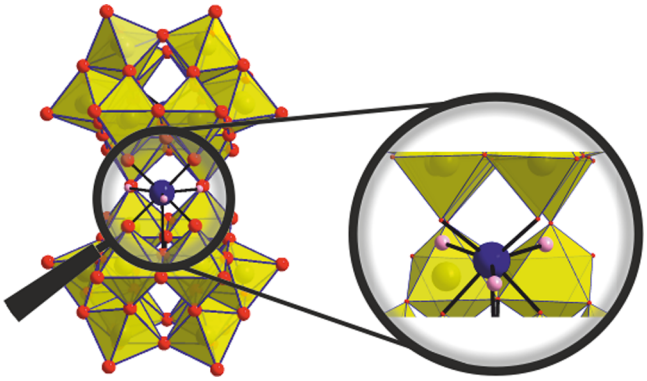

Figure 1. Crystal structure of $[\mathbf{M(H_2O)_3(GeW_{10})_2}]^{n-}$ (n = 9 for M = Ce^{III}, Nd^{III}, Er^{III}; n = 8 for M = Zr^{IV}) showing the polyhedral frontal view of the anion with the three aqua ligands bound to the corresponding metal. Blue and red spheres represent the M - and oxygen ions, respectively. Orange for Ge^{IV} and yellow polyhedra for {WO_6}.

Besides XRD, all five compounds were characterized by ATR-IR spectroscopy (Figure S1) showing the terminal W═O and bridging W−O−W vibrations typical for the Keggin-type polyoxotungstate framework. The bands at 1630 and 2960 cm^{-1} are attributed to vibration and deformation bands of tetrabutylammonium methylene groups.

The number of water molecules and crystal solvents in the compounds $TBA_7H_2[Ce(H_2O)_3(GeW_{10}O_{35})_2]\cdot 3(CH_3)_2CO$ (Figure S5), $TBA_7H_2[Nd(H_2O)_3(GeW_{10}O_{35})_2]\cdot 3(CH_3)_2CO$ (Figure S6), $TBA_7H_2[Er(H_2O)_3(GeW_{10}O_{35})_2]\cdot 3(CH_3)_2CO$ (Figure S7), and $TBA_6H_2[Zr(H_2O)_3(GeW_{10}O_{35})_2]\cdot 3(CH_3)_2CO$ (Figure S8) was determined using thermogravimetric analysis (TGA). All compounds exhibit, in general, three weight-loss regions (Tables S3−S6) that are attributed to losses of three water ligands, acetone and tetrabutylammonium (TBA) molecules, respectively.

The UV/vis spectra of all five polyanions are characterized by an absorption maximum at 275 nm attributed to the $p_\pi(O_b) \rightarrow d_\pi^*(W)$ ligand-to-metal charge-transfer typical for the Keggin-type framework (Figures S10, S11).[36]

Hydrolytic Studies. When compared to other lanthanide substituted POMs, the cerium containing representatives are known to be the most active phosphoesterases due to their higher Lewis acidity and sterically less hindered Lewis acid sites.[37] To test $[\mathbf{Ce(H_2O)_3(GeW_{10})_2}]^{9-}$ and $[\mathbf{Zr(H_2O)_3(GeW_{10})_2}]^{8-}$ toward their potential phosphoesterase activity, NPP as a model substrate was applied. The hydrolytic activity of $[\mathbf{Ce(H_2O)_3(GeW_{10})_2}]^{9-}$ and $[\mathbf{Zr(H_2O)_3(GeW_{10})_2}]^{8-}$ toward NPP was monitored using ^{1}H NMR measurements on reaction mixtures of the corresponding POM (0.5 mM) and NPP (1 mM) in D_2O at pD = 7.0 and 60 °C (Figures 2, S12) considering the high stability of the phosphoester bond present in NPP ($t_{1/2}$ = 135 days at 50 °C) and to create reaction conditions which are comparable to other literature reported reaction systems.[39] The NMR spectra taken after 45, 1200, 1800, 2680, 3790, 5460, and 5580 min of incubation reveal a gradual disappearance of the doublets corresponding to NPP, while two new doublets assigned to the hydrolysis product nitrophenol (NP) are observed (Figure 2, Scheme S1). The upfield shift of the NP peaks can be explained by the hydroxyl group in NP (Figures 2, S12). Based on the ^{1}H NMR integration values, the percentage of NPP after reaction with $[\mathbf{Ce(H_2O)_3(GeW_{10})_2}]^{9-}$ or $[\mathbf{Zr(H_2O)_3(GeW_{10})_2}]^{8-}$ was calculated. The natural logarithm of

https://dx.doi.org/10.1021/acs.inorgchem.0c01852
Inorg. Chem. 2020, 59, 14078−14084

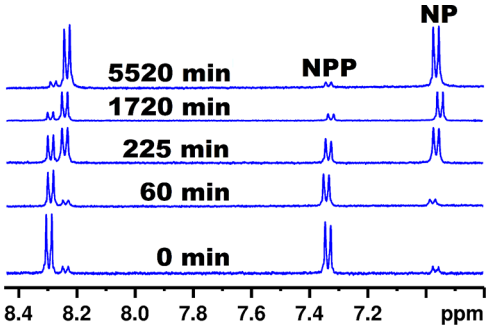

Figure 2. ^{1}H NMR spectra of the hydrolysis of 4-nitrophenylphosphate (NPP) [1 mM] to nitrophenol (NP) with [**Zr**-$(H_2O)_3(GeW_{10}O_{35})_2]^{8-}$ [0.5 mM] in D_2O at pD 7.0 and 60°.

the NPP concentration obtained from the integration values as a function of time fitted to a first-order decay function gave a rate constant of k_{obs} = 3.70 (±0.20) × 10^{-4} min^{-1} for $[Ce(H_2O)_3(GeW_{10})_2]^{9-}$ (Figure S13). To correct for the autohydrolysis of NPP, reaction mixtures lacking the POM were prepared and measured under the same reaction conditions. The rate constant determined from these experiments (k_{uncat} = 2.60 (±0.10) × 10^{-5} min^{-1}) was subtracted from the rate constant (k_{obs} = 3.70 (±0.20) × 10^{-4} min^{-1}) obtained from the experiments investigating $[Ce(H_2O)_3(GeW_{10})_2]^{9-}$ to give the corrected constant (k_{corr}) with a value of 3.44 (±0.30) × 10^{-4} min^{-1}, which is almost an order of magnitude acceleration as compared to the rate of spontaneous hydrolysis of NPP and more than five times higher than other monosubstituted Ln(III) Keggin-type POTs like $[Me_2NH_2]_{11}[Ce^{III}(PW_{11}O_{39})_2]$ (k = 6.72 × 10^{-5} min^{-1}) and $K_4[EuPW_{11}O_{39}]$ (k = 6.42 × 10^{-5} min^{-1}), whereas a comparable value can be observed for $[Me_2NH_2]_{10}[Ce^{IV}(PW_{11}O_{39})_2]$ (k = 3.19 × 10^{-4} min^{-1}) under similar reaction conditions.[19] The comparatively high Lewis activity of $[Ce(H_2O)_3(GeW_{10})_2]^{9-}$ can be explained by the thermodynamically unfavored structural conversion of the dimeric $[Ce^{III/IV}(PW_{11}O_{39})_2]^{10-/9-}$ POM to the monomeric $[Ce^{III/IV}PW_{11}(H_2O)_2]^{4-/3-}$ species, which is a crucial step in order to be hydrolytically active[18] (Scheme S3), whereas the architecture of $[Ce(H_2O)_3(GeW_{10})_2]^{9-}$ exhibits a freely accessible Lewis acid metal center without structural conversion (Figure 1). As for $[Zr(H_2O)_3(GeW_{10})_2]^{8-}$, a corrected rate constant of k_{corr} = 5.36 (±0.05) × 10^{-4} min^{-1} is observed (Figure S15), which is comparable to other monosubstituted Zr^{IV} compounds such as $K_{15}H[Zr(\alpha_2$-$P_2W_{17}O_{61})_2]$ (k_{corr} = 7.56 × 10^{-4} min^{-1}) under similar conditions.[38] This value is 1.5 times higher than the value observed for $[Ce(H_2O)_3(GeW_{10})_2]^{9-}$ and 3.4 times higher than the corrected rate constant observed for the $[GeW_{10}O_{36}]^{8-}$ precursor (k_{corr} = 1.59 × 10^{-4} min^{-1}) (Figure S16), which can be attributed to the higher Lewis acid activity of Zr^{IV}. The pD value of the reaction mixtures after reaction was measured thereby remaining almost unchanged (pD 7.0, start vs pD 6.8, end of experiment).

The removal of toxic organophosphorus (OP) nerve agents and pesticides remains a significant and general goal which is mainly achieved by hydrolytically transforming the toxic OP compounds into nontoxic forms. Considering the structural similarity between NPP and *O*,*O*-dimethyl *O*-(4-nitrophenyl) phosphate (DMNP), which is an established OP ester nerve simulant,[25] hydrolytic studies on the degradation performance of $[Zr(H_2O)_3(GeW_{10})_2]^{8-}$, exhibiting both the highest water solubility and phosphoesterase activity expressed by 24 times the accelerated hydrolysis of the relatively inert phosphoester bond present in NPP, were performed at room temperature (25 °C) and physiological pH (125 mM Tris-HCl, pH 7) (Scheme S2). A buffered reaction system was chosen considering the *in situ* formation of the acidic product dimethyl phosphate (DMP). The stepwise hydrolysis of DMNP to nitrophenol was monitored with ^{31}P NMR spectroscopy by taking aliquots after 180, 1400, 1524 1614, and 2940 min of reaction (Figure 3). A stepwise disappearance

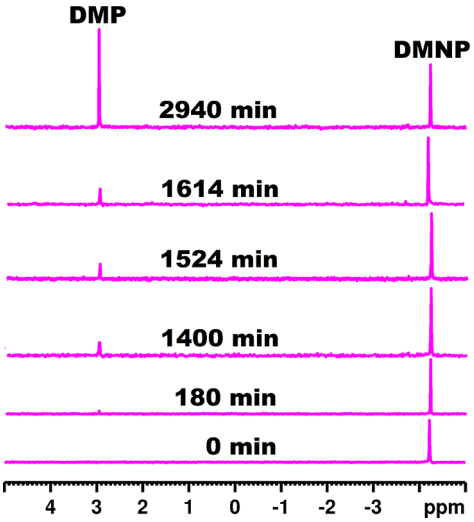

Figure 3. ^{31}P NMR spectra of the hydrolysis of DMNP [4.2 mM] to nitrophenol (NP) and dimethyl phosphate (DMP) with [**Zr**-$(H_2O)_3(GeW_{10}O_{35})_2]^{8-}$ [2.5 mM] in Tris-HCl [125 mM]/D_2O (50%) at pD 7.0 and room temperature (25 °C).

of the singlet corresponding to the substrate DMNP and gradual appearance of a singlet attributed to the hydrolysis side product dimethyl phosphate (DMP) can be observed (Figure 3).[28] The corrected rate constant after subtracting the rate constant obtained from reaction mixtures lacking the POM catalyst (k_{uncat} = 4.01 (±0.10) × 10^{-5} min^{-1}) - under elsewise identical reaction conditions considering autohydrolysis of the substrate - gives a value of k_{corr} = 2.42 (±0.10) × 10^{-4} min^{-1} (Figure S17) which is about seven times higher than the values obtained for the uncatalyzed reaction (k_{uncat} = 4.01 (±0.10) × 10^{-5} min^{-1}) and control experiments containing the $[GeW_{10}O_{36}]^{8-}$ precursor (k_{corr} = 3.37 (±0.12) × 10^{-5} min^{-1}) (Figure S18), respectively. Concentration dependent experiments on the phosphoesterase activity of $[Ce(H_2O)_3(GeW_{10})_2]^{9-}$ and $[Zr(H_2O)_3(GeW_{10})_2]^{8-}$ toward NPP and DMNP were carried out, and the substrate conversion for a specific reaction time (45.6 h, 49 h, and 25 h) under varying catalyst concentrations (0.5 mM, 1.0 mM, 1.25 mM, 2.5 mM) was recorded and compared (Table S20).

Solution stability studies on $[Ce(H_2O)_3(GeW_{10})_2]^{9-}$ and $[Zr(H_2O)_3(GeW_{10})_2]^{8-}$ after reaction with NPP and DMNP were intended to be performed; however, due to the low solubility and sensitivity of the ^{183}W nucleus (14.3% natural abundance), the ^{183}W NMR measurements at conditions pertinent to the catalytic reactions were not very informative, which is a common problem encountered in POM chemistry.[39] Considering the low solubility of the polyanion, the POM concentrations used for the hydrolysis experiments were too

https://dx.doi.org/10.1021/acs.inorgchem.0c01852
Inorg. Chem. 2020, 59, 14078−14084

low to obtain reasonable amounts for consecutive postcatalytic PXRD measurements. Hence, to prove stability of $[Ce(H_2O)_3(GeW_{10})_2]^{9-}$ and $[Zr(H_2O)_3(GeW_{10})_2]^{8-}$ indirectly, the IR spectra of the polyanions were recorded after precipitation with tetrabutylammonium bromide, thereby clearly showing the characteristic W−O−W bridging and terminal W═O vibrations in the tungsten fingerprint area from 300−1000 cm^{-1}, which proves the solution stability of the polyanions after reaction with NPP (Figures S2, S3) and DMNP, respectively (Figure S4), and represents an established method frequently used in POM chemistry.[39] Subsequent control experiments with $CeCl_3$ and $ZrOCl_2$ as nonshielded free Lewis metal centers resulted in the formation of precipitates or insoluble Zr(IV) hydroxyl polymeric gels, respectively, shown by the disappearance of the ^1H NMR peaks even at low concentrations of the corresponding metal center, which additionally proves the solution stability of the POM compounds under reaction conditions (Figure S14).[40−42] The recyclability of $[Zr(H_2O)_3(GeW_{10})_2]^{8-}$ as a catalyst for the decontamination of DMNP was tested in a consecutive experiment by reloading the reaction mixture with DMNP substrate after ^{31}P NMR measurements confirmed that 97% of DMNP was converted to the hydrolysis product DMP (Figure S19). A direct comparison of the turnover frequency (TOF) values obtained for $[Zr(H_2O)_3(GeW_{10})_2]^{8-}$ in the first and the second reaction cycle indicates no change in the catalytic performance of the polyanion after reaction (TOF = 0.02 h^{-1}) (Table S18).

Antibacterial Studies. The antibacterial activity of the water-soluble polyanions $[Ce(H_2O)_3(GeW_{10})_2]^{9-}$ and $[Zr(H_2O)_3(GeW_{10})_2]^{8-}$ of the compound series was tested against *M. catarrhalis* at physiological pH (Tables S21, S22). The minimum inhibitory concentration (MIC) of $[Ce(H_2O)_3(GeW_{10})_2]^{9-}$ is compared to that of $Ce(NO_3)_3$ and the lacunary GeW_{10} unit. $[Ce(H_2O)_3(GeW_{10})_2]^{9-}$ exhibits better antibacterial activity (MIC value of 32 μg/mL) compared to the lacunary building block GeW_{10} (MIC = 64 μg/mL), whereas $Ce(NO_3)_3$ shows no inhibition activity (MIC > 256 μg/mL) (Table S21). As for $[Zr(H_2O)_3(GeW_{10})_2]^{8-}$, no difference in the antibacterial activity between $[Zr(H_2O)_3(GeW_{10})_2]^{8-}$ and $ZrO(NO_3)_2$ is observed as both the $[Zr(H_2O)_3(GeW_{10})_2]^{8-}$ polyanion and $ZrO(NO_3)_2$ exhibit an inhibitory effect (Table S22). It can be concluded that the encapsulation of the Lewis acidic metal centers using POM lacunary ligands thereby forming the negatively charged sandwich-POM species led to enhanced antibacterial properties of the otherwise inactive Ce^{3+} metal center, whereas the activity observed for $ZrO(NO_3)_2$ can be most likely explained by the strong oxidizing properties of the salt itself.

CONCLUSIONS

In conclusion, the combination of the $(TBA)[GeW_{10}]$ precursor with lanthanides in organic medium afforded a versatile synthetic route for the preparation of monosubstituted 4f-doped germanotungstates exemplified by the successful incorporation of early (Ce^{III}, Nd^{III}), mid (Gd^{III}), and late (Er^{III}) lanthanides at room temperature. Addition of hydrogen peroxide to the reaction system expands the synthetic route to 4d-substituted germanotungstates shown by the crystallization and characterization of the zirconium(IV) containing counterpart. Systematic studies on the phosphoesterase activity of the water-soluble polyanions $[Ce(H_2O)_3(GeW_{10})_2]^{9-}$ and $[Zr(H_2O)_3(GeW_{10})_2]^{8-}$ revealed that $[Zr(H_2O)_3(GeW_{10})_2]^{8-}$ is a highly active recyclable catalyst for the Lewis acidic degradation of the nerve agent simulant DMNP. Antibacterial studies toward *M. catarrhalis* revealed that the highly negatively charged polyanion $[Ce(H_2O)_3(GeW_{10})_2]^{9-}$ exhibits inhibitory properties (MIC = 32 μg/mL) in contrast to $Ce(NO_3)_3$ (MIC > 256 μg/mL). These results exemplify the potential of the underinvestigated POM reaction systems in organic media to apply lacunary POM ligands for the successful encapsulation of Lewis acid metal centers further enhancing their catalytic and antibacterial activity which opens perspectives for the tailored design of model compounds with biotechnologically relevant applications.

ASSOCIATED CONTENT

Supporting Information

The Supporting Information is available free of charge at https://pubs.acs.org/doi/10.1021/acs.inorgchem.0c01852.

Details on synthesis, IR, TGA, XRD, UV−vis, and NMR measurements (PDF)

Accession Codes

CCDC 1915316−1915318, 1915355, and 2010882 contain the supplementary crystallographic data for this paper. These data can be obtained free of charge via www.ccdc.cam.ac.uk/data_request/cif, or by emailing data_request@ccdc.cam.ac.uk, or by contacting The Cambridge Crystallographic Data Centre, 12 Union Road, Cambridge CB2 1EZ, UK; fax: +44 1223 336033.

AUTHOR INFORMATION

Corresponding Author

Annette Rompel − *Fakultät für Chemie, Institut für Biophysikalische Chemie, Universität Wien, 1090 Wien, Austria*; orcid.org/0000-0002-5919-0553; Email: annette.rompel@univie.ac.at; www.bpc.univie.ac.at

Authors

Elias Tanuhadi − *Fakultät für Chemie, Institut für Biophysikalische Chemie, Universität Wien, 1090 Wien, Austria*

Emir Al-Sayed − *Fakultät für Chemie, Institut für Biophysikalische Chemie, Universität Wien, 1090 Wien, Austria*

Alexander Roller − *Fakultät für Chemie, Zentrum für Röntgenstrukturanalyse, Universität Wien, 1090 Wien, Austria*

Hana Cipčić-Paljetak − *Center for Translational and Clinical Research, Croatian Center of Excellence for Reproductive and Regenerative Medicine, School of Medicine, University of Zagreb, 10000 Zagreb, Croatia*

Donatella Verbanac − *Faculty of Pharmacy and Biochemistry, University of Zagreb, 10000 Zagreb, Croatia*

Complete contact information is available at: https://pubs.acs.org/10.1021/acs.inorgchem.0c01852

Notes

The authors declare no competing financial interest.

ACKNOWLEDGMENTS

Nuclear magnetic resonance (NMR) measurements were performed by Ricarda Bugl and Sabine Schneider at the NMR center, Faculty of Chemistry, University of Vienna. The authors wish to thank Dr. Ioannis Kampatsikas, Nadiia Gumerova, Ph.D., Dipl.-Ing. Matthias Pretzler, and Dr. Joscha

Breibeck for valuable discussions concerning this work and Ass.-Prof. Dr. Peter Unfried for TGA measurements. We gratefully acknowledge the Austrian Science Fund FWF (P27534 and P33089) as well as the University of Vienna for financial support. E.T. and A.R. acknowledge the University of Vienna for awarding an Uni:docs fellowship to E.T. Bilateral financial funding is provided by the Centre for International Cooperation & Mobility (ICM) of the Austrian Agency for International Cooperation in Education and Research (OeAD-GmbH) Project No. HR 06/2020 to A.R. and the Project "Biological profiling of polyoxometalates" to H.C.P.

REFERENCES

(1) Pope, M. T. In *Heteropoly and Isopoly Oxometalates*; Springer: Berlin, 1983; pp 15−18.
(2) Bösing, M.; Nöh, A.; Loose, I.; Krebs, B. Highly Efficient Catalysts in Directed Oxygen-Transfer Processes: Synthesis, Structures of Novel Manganese-Containing Heteropolyanions, and Applications in Regioselective Epoxidation of Dienes with Hydrogen Peroxide. *J. Am. Chem. Soc.* **1998**, *120* (29), 7252−7259.
(3) Wang, S. S.; Yang, G. Y. Recent Advances in Polyoxometalate-Catalyzed Reactions. *Chem. Rev.* **2015**, *115*, 4893−4962.
(4) Sadakane, M.; Steckhan, E. Electrochemical Properties of Polyoxometalates as Electrocatalysts. *Chem. Rev.* **1998**, *98* (1), 219−238.
(5) Clemente-Juan, J. M.; Coronado, E.; Arino, A. G. Magnetic polyoxometalates: from molecular magnetism to molecular spintronics and quantum computing. *Chem. Soc. Rev.* **2012**, *41*, 7464−7478.
(6) Bijelic, A.; Aureliano, M.; Rompel, A. The antibacterial activity of polyoxometalates: structures, antibiotic effects and future perspectives. *Chem. Commun.* **2018**, *54*, 1153−1169.
(7) (a) Bijelic, A.; Aureliano, M.; Rompel, A. Polyoxometalates as Potential Next-Generation Metallodrugs in the Combat Against Cancer. *Angew. Chem., Int. Ed.* **2019**, *58*, 2980−2999. (b) Bijelic, A.; Aureliano, M.; Rompel, A. Im Kampf gegen Krebs: Polyoxometallate als nächste Generation metallhaltiger Medikamente. *Angew. Chem.* **2019**, *131*, 3008−3029.
(8) Bijelic, A.; Rompel, A. The use of polyoxometalates in protein crystallography - An attempt to widen a well-known bottleneck. *Coord. Chem. Rev.* **2015**, *299*, 22−38.
(9) Bijelic, A.; Rompel, A. Ten Good Reasons for the Use of the Tellurium-Centered Anderson-Evans Polyoxotungstate in Protein Crystallography. *Acc. Chem. Res.* **2017**, *50*, 1441−1448.
(10) Bijelic, A.; Rompel, A. Polyoxometalates - More than a phasing tool in protein crystallography. *ChemTexts* **2018**, *4*, 10.
(11) Dolbecq, A.; Dumas, E.; Mayer, C. R.; Mialane, P. Hybrid Organic-Inorganic Polyoxometalate Compounds: From Structural Diversity to Applications. *Chem. Rev.* **2010**, *110* (10), 6009−6048.
(12) Ma, X.; Li, H.; Chen, L.; Zhao, J. The main progress over the past decade and future outlook on high-nuclear transition-metal substituted polyoxotungstates: from synthetic strategies, structural features to functional properties. *Dalton Trans.* **2016**, *45*, 4935−4960.
(13) Sato, R.; Suzuki, K.; Minato, T.; Yamaguchi, K.; Mizuno, N. Sequential Synthesis of 3d-3d′-4f Heterometallic Heptanuclear Clusters in between Lacunary Polyoxometalates. *Inorg. Chem.* **2016**, *55* (5), 2023−2029.
(14) Hanaya, T.; Suzuki, K.; Sato, R.; Yamaguchi, K.; Mizuno, N. Creation of bismuth-tungsten oxide nanoclusters using lacunary polyoxometalates. *Dalton Trans.* **2017**, *46*, 7384−7387.
(15) Sugahara, K.; Kimura, T.; Kamata, K.; Yamaguchi, K.; Mizuno, N. A highly negatively charged γ-Keggin germanodecatungstate efficient for Knoevenagel condensation. *Chem. Commun.* **2012**, *48*, 8422−8424.
(16) Geletii, Y. V.; Hill, C. L.; Musaev, D. G. An All-Inorganic, Stable, and Highly Active Tetraruthenium Homogeneous Catalyst for Water Oxidation. *Angew. Chem., Int. Ed.* **2008**, *47*, 3896−3899.
(17) Boglio, C.; Micoine, K.; Remy, P.; Hasenknopf, B.; Thorimbert, S.; Lacote, E.; Malacria, M.; Afonso, C.; Tabet, J. C. Increased Lewis Acidity in Hafnium-Substituted Polyoxotungstates. *Chem. - Eur. J.* **2007**, *13*, 5426−5432.
(18) Luong, T. K. N.; Mihaylov, T. T.; Absillis, G.; Shestakova, P.; Pierloot, K.; Parac-Vogt, T. N. Phosphate Ester Bond Hydrolysis Promoted by Lanthanide-Substituted Keggin-type Polyoxometalates Studied by a Combined Experimental and Density Functional Theory Approach. *Inorg. Chem.* **2016**, *55* (19), 9898−9911.
(19) Hegg, E.; Burstyn, J. N. Toward the development of metal-based synthetic nucleases and peptidases: a rationale and progress report in applying the principles of coordination chemistry. *Coord. Chem. Rev.* **1998**, *173*, 133−165.
(20) Salvio, R.; Volpi, S.; Folcarelli, T.; Casnatic, A.; Cacciapaglia, R. Ribonuclease Activity of an Artificial Catalyst That Combines a Ligated Cu^{II} Ion and a Guanidinium Group at the Upper Rim of a cone-Calix[4]arene Platform. *J. Org. Chem.* **2015**, *80* (11), 5887−5893.
(21) Chin, J. Artificial dinuclear phosphoesterases. *Curr. Opin. Chem. Biol.* **1997**, *1*, 514−521.
(22) Lippert, B. From cisplatin to artificial nucleases — the role of metal ion-nucleic acid interactions in biology. *BioMetals* **1992**, *5*, 195−208.
(23) Das, B.; Daver, H.; Pyrkosz-Bulska, M.; Gumienna-Kontecka, E.; Himo, F.; Nordlander, E. An Unsymmetric Ligand with a N_5O_2 Donor Set and Its Corresponding Dizinc Complex: A Structural and Functional Phosphoesterase Model. *Eur. J. Inorg. Chem.* **2018**, 4004−4013.
(24) Raja, K.; Susseelamma, A.; Reddy, K. H. Synthesis, spectral properties and DNA binding and nuclease activity of lanthanide (III) complexes of 2-benzoylpyridine benzhydrazone: X-ray crystal structure, Hirshfeld studies and nitrate-π interactions of cerium (III) complex. *J. Chem. Sci.* **2016**, *128*, 23−35.
(25) Jang, Y. J.; Kim, K.; Tsay, O. G.; Atwood, D. A.; Churchill, D. G. Update 1 of: Destruction and Detection of Chemical Warfare Agents. *Chem. Rev.* **2015**, *115*, PR1−PR76.
(26) Balow, R. B.; Lundin, J. G.; Daniels, G. C.; Gordon, W. O.; McEntee, M.; Peterson, G. W.; Wynne, J. H.; Pehrsson, P. E. Environmental Effects on Zirconium Hydroxide Nanoparticles and Chemical Warfare Agent Decomposition: Implications of Atmospheric Water and Carbon Dioxide. *ACS Appl. Mater. Interfaces* **2017**, *9*, 39747−39757.
(27) Ebrahim, A. M.; Plonka, A. M.; Tian, Y.; Senanayake, S. D.; Gordon, W. O.; Balboa, A.; Wang, H.; Collins-Wildman, D. L.; Hill, C. L.; Musaev, D. G.; Morris, J. R.; Troya, D.; Frenkel, A. I. Multimodal Characterization of Materials and Decontamination Processes for Chemical Warfare Protection. *ACS Appl. Mater. Interfaces* **2020**, *12*, 14721−14738.
(28) Collins-Wildman, D. L.; Kim, M.; Sullivan, K. P.; Plonka, A. M.; Frenkel, A. I.; Musaev, D. G.; Hill, C. L. Buffer-Induced Acceleration and Inhibition in Polyoxometalate-Catalyzed Organophosphorus Ester Hydrolysis. *ACS Catal.* **2018**, *8*, 7068−7076.
(29) Zhang, D.; Zhang, W.; Lin, Z.; Dong, J.; Zhen, N.; Chi, Y.; Hu, C. Mono- and Di-Sc-Substituted Keggin Polyoxometalates: Effective Lewis Acid Catalysts for Nerve Agent Simulant Hydrolysis and Mechanistic Insights. *Inorg. Chem.* **2020**, *59*, 9756−9764.
(30) Tajima, Y. The effects of tungstophosphate and tungstosilicate on various stress promoters transformed in *Escherichia coli*. *J. Inorg. Biochem.* **2003**, *94*, 155−160.
(31) Inoue, M.; Segawa, K.; Matsunaga, S.; Matsumoto, N.; Oda, M.; Yamase, T. Antibacterial activity of highly negative charged polyoxotungstates, $K_{27}[KAs_4W_{40}O_{140}]$ and $K_{18}[KSb_9W_{21}O_{86}]$, and Keggin-structural polyoxotungstates against *Helicobacter pylori*. *J. Inorg. Biochem.* **2005**, *99*, 1023−1031.
(32) Karalus, R.; Campagnari, A. *Moraxella catarrhalis*: a review of an important human mucosal pathogen. *Microbes Infect.* **2000**, *2*, 547−559.

https://dx.doi.org/10.1021/acs.inorgchem.0c01852
Inorg. Chem. 2020, 59, 14078−14084

(33) Gumerova, N. I.; Al-Sayed, E.; Krivosudský, L.; Čipčić-Paljetak, H.; Verbanac, D.; Rompel, A. Antibacterial activity of polyoxometalates against *Moraxella catarrhalis*. *Front. Chem.* **2018**, *6*, 336.
(34) Bassil, B.; Kortz, U. Divacant polyoxotungstates: Reactivity of the gamma-decatungstates $[\gamma\text{-}XW_{10}O_{36}]^{8-}$ (X = Si, Ge). *Dalton Trans.* **2011**, *40*, 9649−9661.
(35) Sommers, J. A.; Hutchison, D. C.; Martin, N. P.; Kozma, K.; Keszler, D. A.; Nyman, M. Peroxide-Promoted Disassembly Reassembly of Zr-Polyoxocations. *J. Am. Chem. Soc.* **2019**, *141* (42), 16894−16902.
(36) Bi, L.; Li, B.; Wu, L.; Bao, Y. Synthesis, characterization and crystal structure of a novel 2D network structure based on hexacopper(II) substituted tungstoantimonate. *Inorg. Chim. Acta* **2009**, *362*, 3309−3313.
(37) Suzuki, K.; Sugawa, M.; Kikukawa, Y.; Yamata, K.; Yamaguchi, K.; Mizuno, N. Strategic Design and Refinement of Lewis Acid-Base Catalysis by Rare-Earth-Metal-Containing Polyoxometalates. *Inorg. Chem.* **2012**, *51*, 6953−6961.
(38) Vanhaecht, S.; Absillis, G.; Parac-Vogt, T. N. Hydrolysis of DNA model substrates catalyzed by metal-substituted Wells-Dawson polyoxometalates. *Dalton Trans.* **2012**, *41*, 10028−10034.
(39) Kandasamy, B.; Vanhaecht, S.; Nkala, F. M.; Beelen, T.; Bassil, B. S.; Parac-Vogt, T. N.; Kortz, U. Gallium(III)-Containing, Sandwich-Type Heteropolytungstates: Synthesis, Solution Characterization, and Hydrolytic Studies toward Phosphoester and Phosphoanhydride Bond Cleavage. *Inorg. Chem.* **2016**, *55*, 9204−9211.
(40) Luong, T. K. N.; Absillis, G.; Shestakova, P.; Parac-Vogt, T. N. Hydrolysis of the RNA model substrate catalyzed by a binuclear Zr^{IV}-substituted Keggin polyoxometalate. *Dalton Trans.* **2015**, *44*, 15690−15696.
(41) Singhal, A.; Toth, L. M.; Lin, J. S.; Affholter, K. Zirconium(IV) Tetramer/Octamer Hydrolysis Equilibrium in Aqueous Hydrochloric Acid Solution. *J. Am. Chem. Soc.* **1996**, *118*, 11529−11534.
(42) Moss, R. A.; Zhang, J.; Ragunathan, K. G. Zirconium and hafnium cations rapidly cleave model phosphodiesters in acidic aqueous solutions. *Tetrahedron Lett.* **1998**, *39*, 1529−1532.

https://dx.doi.org/10.1021/acs.inorgchem.0c01852
Inorg. Chem. 2020, 59, 14078−14084